https://www.scirp.org/journal/jbise
Journal of Biomedical Science and Engineering, 2026, Vol. 19, (No. 6), pp: 227-241

Numerical Simulation of the Mitral Valve Repair

Tévy Julie Pigeon[1], Pascale Kulisa[2], Fabrice Morestin[1], Benyebka Bou-Saïd[1]

[1]INSA Lyon, CNRS, LaMCoS, Villeurbanne, France; [2]Univ Lyon, INSA Lyon, Ecole Centrale de Lyon, Claude Bernard Univ Lyon 1, CNRS, LMFA, Villeurbanne, France

Correspondence to: Tévy Julie Pigeon, tevy.pigeon@insa-lyon.fr
Keywords: Annuloplasty Device, Biomechanics, Finite Element Method, Native Annulus, Percutaneous Surgery
Received: March 30, 2026 **Accepted:** June 23, 2026 **Published:** June 25, 2026

ABSTRACT

This paper presents a customizable finite element framework of the mitral valve and surrounding structures for the numerical study of transcatheter annuloplasty. The geometry used in this work corresponds to a single reference left-heart model provided by KIT and was preprocessed using CAD tools. The present study focuses on the mechanical response of the valve region during prosthetic ring positioning and annular downsizing. In the complete annuloplasty model, prosthesis positioning and downsizing were completed sequentially in Abaqus. Because severe mesh distortion prevented completion of physiological loading after downsizing in the prosthesis-including model, ventricular contraction and pressure loading were implemented in a separate "Physio" configuration without the prosthesis. The resulting deformation and stress patterns are consistent with previously reported computational trends, with elevated stresses in the atrioventricular-junction region near the fibrous trigones and posterior annular region. The model should therefore be considered a methodological framework and proof of concept, rather than a fully validated patient-specific planning tool. Future work will focus on mesh convergence, experimental validation, and reintegration of physiological loading into the complete annuloplasty model.

1. INTRODUCTION

1.1. Clinical Context

Cardiovascular disease remains the leading cause of death worldwide, accounting for 31% of all global deaths. Mitral regurgitation (MR) is the second most prevalent valve disorder in Europe, affecting 2% of the global population [1]. This pathology is characterized by an enlargement of the mitral valve (MV) diameter, which compromises the coaptation of the leaflets during systole. Consequently, a leak in the valve allows retrograde blood flow from the left ventricle into the left atrium. First introduced by Alain Carpentier in

1983 [2], annuloplasty is a surgical technique aimed at reducing the mitral valve's diameter and stabilizing the repair through the implantation of a prosthetic ring. This ring is anchored to the native annulus using nitinol threads or surgical anchors. Despite being regarded as the gold standard for the surgical repair of pathological valve [3], open-heart annuloplasty remains a highly invasive procedure, often unsuitable for high-risk patients. In contrast, transcatheter techniques, considered minimally invasive, allow surgeons to operate internally without halting cardiac function [4]. One such approach, MitraClip®, addresses MR by clamping the leaflets together. Our study focuses on transcatheter annuloplasty, with particular attention to prosthetic durability. The Cardioband® is another minimally invasive annuloplasty device. It features a flexible anchoring system that accommodates various mitral annulus geometries [5]. Parametric and numerical simulations of the Cardioband on patient-specific anatomies [6], along with experimental campaigns on anchor dehiscence [7], have been conducted. Nevertheless, despite obtaining CE certification, the device has not achieved widespread success [8].

1.2. A Personalized Model

The leading cause of short-term failure and subsequent re-operation following annuloplasty is anchor dehiscence [3]. The mechanical and hemodynamic stresses exerted on the system, the healing process at the anchor sites, the local collagen density [3, 9], and the mechanical properties of the prosthesis: all influence this failure mode. These factors vary significantly among patients. Therefore, a personalized, patient-specific numerical model is essential to simulate the procedure virtually and determine optimal anchoring parameters such as location, orientation, and quantity tailored to the patient's valve anatomy.

1.3. Study Objectives

Our objective is to develop a digital twin of the mitral valve and surrounding structures to support patient-specific prosthetic ring design. The first phase involves a finite element model to assess tissue stress after anchor implantation. Later phases will incorporate growth, remodeling, and fatigue to evaluate long-term prosthesis viability. A finite element approach was selected to address this solid mechanics problem. The present work is intended as a methodological step toward patient-tailored annuloplasty simulation. Its main contribution is the construction of a continuous atrio-ventriculo-valvular finite element geometry coupled with an idealized annuloplasty ring and discrete anchoring regions, allowing stress localization to be assessed during prosthesis positioning and downsizing. At this stage, the framework is not presented as a validated clinical prediction tool; rather, it provides a basis for future mesh refinement, experimental validation, and patient-specific adaptation.

2. STATE OF ART

2.1. Functional Anatomy of the Mitral Valve

The mitral annulus is essential for annuloplasty implantation, providing structural stability at the junction of the left atrium, left ventricle, and mitral leaflets. It is composed of discontinuous fibrous tissues with variable thickness and density, although its anatomy and mechanics remain incompletely understood [10], [11]. Anteriorly, it forms part of the heart's fibrous skeleton, with the fibrous trigones serving as key anchoring points for the first and last prosthetic sutures [12]. Posteriorly, the annulus is less well defined and may coincide with the atrioventricular junction, merge with the leaflet hinge, lie slightly below it, or be nearly absent; histologically, it includes muscular, fibrous, and adipose tissue [10]. The mitral valve is also supported by papillary muscles and chordae tendineae, which prevent leaflet prolapse into the left atrium during systole [13].

2.2. Previous Numerical Models

Over the past 15 years, computational models have significantly advanced the understanding of left heart and mitral valve biomechanics.

Wong *et al.* [14] extended the work of Wenk *et al.* [15] by incorporating annuloplasty into their model of an infarcted left ventricle, with valve leaflets reconstructed from B-spline curves fitted to points derived from magnetic resonance images and a mitral annulus defined by 12 points along the valve perimeter.

Similarly, Kong *et al.* [16] developed an infarcted left ventricular model with leaflets reconstructed from multi-slice CT images. They analyzed the effect of a prosthetic ring on leaflet coaptation and chordae tendineae tension following papillary muscle relocation.

Gao [17] developed a comprehensive FSI model of the mitral valve, incorporating a simplified atrium, ventricle, and aortic outflow. Valve geometry was reconstructed from cine MRI, and fibrous structures were modelled using biomarker-segmented features and fiber-reinforced constitutive laws.

Rausch *et al.* [18], using an extended Living Heart Model [19], simulated annuloplasty with 14 sutures. The geometry was derived from Zygote® models and meshed with linear tetrahedral elements. This study quantified stress and strain changes and identified maximal stretch regions near the aorto-mitral junction and posterolateral annulus.

2.3. Limitations of Existing Studies

Most existing models either oversimplify or omit the mitral annular region, often representing it only through the leaflet-ventricle interface. In the present model, the anatomical annulus is not segmented as a separate material domain. Instead, the annular region is defined operationally as the atrioventricular junction, corresponding to the continuous transition between the leaflets, atrial base, and ventricular inlet. Therefore, stress values reported in this region should be interpreted as stresses in the annular/junctional region, not as stresses in a separately modeled histological annulus.

3. MATERIAL AND METHODS

3.1. Geometric Reconstruction of the Mitral Valve

The mitral valve and surrounding left-heart geometry used in this study correspond to a single reference anatomical model provided by the Computational Cardiac Modeling group at the Karlsruhe Institute of Technology. The initial segmentation had been performed by an external provider before transfer to the authors. Consequently, the original imaging modality, acquisition parameters, and subject-level metadata were not available to the authors. The model should therefore be regarded as a customizable finite element framework based on one reference anatomy, rather than a fully documented patient-specific model. The reconstructed geometry includes the mitral leaflets, the lower portion of the left atrial cavity, the upper section of the left ventricle, and part of the aortic outflow tract (see **Figure 1**).

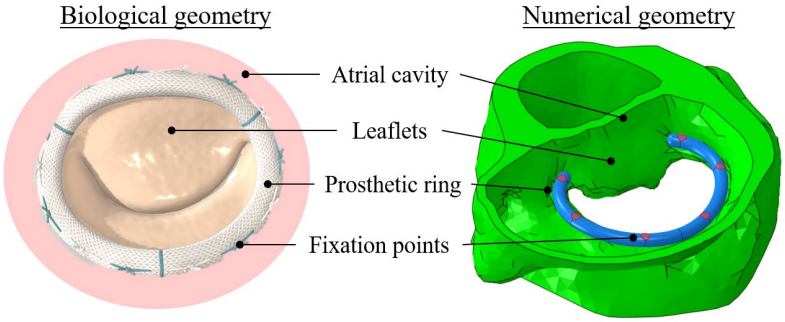

Figure 1. Parallel between the biological mitral valve and the numerical model geometries. Three actors are crucial to model the annuloplasty: the biological tissue (atrium, ventricle, leaflets, in green), the prosthetic ring (blue) and the fixation points (red).

The prosthetic ring used in this study was based on the Carpentier-Edwards Physio Annuloplasty Ring.

It was recreated in Creo Parametric from the 2009 Carpentier patent. A 36-mm ring, with major and minor axes of 36 mm and 25.5 mm and a 3-mm cross-sectional diameter, was modeled to fit the valve geometry (see Figure 2). Anchors were represented by 14 circular surfaces of 1-mm radius, evenly distributed along the ring's free edges and oriented toward the valve wall: parallel, perpendicular, or at 45˚ to the horizontal plane. The first and last anchors were aligned with the fibrous trigones.

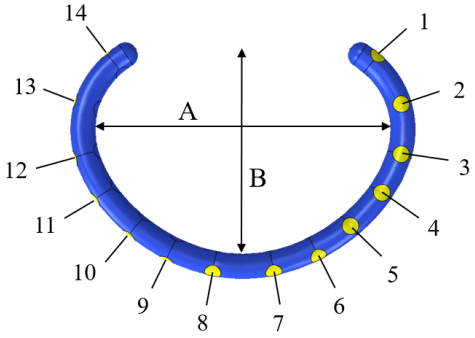

Figure 2. Bottom view of the prosthetic ring (blue) and 14 oriented anchors (yellow). (A) Long axis, (B) minor axis.

3.2. Hypothesis

- The myocardium is fibrous and strongly anisotropic, but for simplicity it is modeled here as an isotropic hyperelastic Neo-Hookean material rather than with a more complex orthotropic law [20].
- Only passive myocardial behavior is modeled explicitly; active contraction is applied through displacement boundary conditions.
- Hemodynamic loading includes static pressure and wall shear stress, but CFD simulations showed that static pressure contributes about five orders of magnitude more to valve and ventricular stress. Therefore, only static pressure is retained. The CFD simulations were performed in OpenFOAM, an open-source CFD software.

3.3. Finite Element Model

This problem of solid mechanics is solved by means of the Finite Elements Method with the commercial code Abaqus 2019 (v16.11.20).

3.3.1. Resolution Scheme, Convergence and Computational Cost

An implicit quasi-static solver was used to obtain accurate peak-systolic stresses, including geometric non-linearities and parallel computation on five CPUs. Each simulation took about one hour.

The mitral valve was meshed with 5 mm quadratic tetrahedral elements, and the prosthesis with similar elements of about 1 mm. The full model contained 79,598 elements and 146,104 nodes.

Because of the valve's geometric complexity, a finer mesh could not be generated, so all simulations used a single mesh. A mesh-convergence study will be needed to optimize the balance between accuracy and computational cost.

3.3.2. Workflow

The numerical workflow was divided into two parts. First, the complete annuloplasty model including the prosthetic ring was used to simulate prosthesis positioning and annular downsizing. Second, because severe mesh distortion prevented physiological loading from being completed after downsizing in the prosthesis-including model, a separate "Physio" configuration without the prosthesis was used to demonstrate ventricular contraction and pressure loading.

• Step 1: Prosthesis positioning by prescribed vertical displacement until contact with the tissue was achieved.

• Step 2: Annular downsizing using the deformed geometry and stress field from Step 1, with tie constraints at the anchoring regions. Prosthesis diameter reduction pilots the native annulus diameter reduction.

• Separate Physio configuration: ventricular contraction and hemodynamic pressure loading without the prosthesis.

Considering the fact that the atrium remains fixed during the systolic phase, a fixed boundary condition is defined on the top surface of the model.

Step 1: Prosthetic Ring Implantation (MEP)

The ring is aligned and pressed against the valve tissue using a prescribed vertical displacement. The resulting geometry is then used for the next phase. For methodological development, vertical springs of 2200 N/m connect leaflet free-edge nodes to the ground. Contact is modeled using general contact with hard normal behavior and defined tangential properties.

Step 2: Annular Downsizing

Surgeons recommend reducing the diameter by 30% to restore valve competence. For the 36-mm ring used here, the imposed 12-mm diameter reduction corresponds to approximately 33% downsizing, close to the clinically targeted order of 30%. This was implemented as a 6-mm radial displacement of the prosthesis

A tie constraint was imposed between the prosthetic anchoring surfaces and the atrial cavity, binding valve nodes to prosthesis ones. This reflects the relative stiffness—biological tissue is assumed to deform more than the prosthesis.

The same general contact definition was applied everywhere except at the anchor points.

Step 3: Post-Surgical Loads—Ventricular Contraction and Hemodynamic Pressure

Severe mesh distortion after downsizing prevented completion of the simulation. An alternative "Physio" model was therefore built from the end of the MEP step, including ventricular contraction and pressure loading but excluding the prosthesis.

Since the mitral valve diameter decreases by about 6 mm during systole [21, 22], ventricular contraction was modeled as a 3 mm radial displacement at the ventricular base. Tendinous chords were represented by 2200 N/m springs [23, 24] connecting leaflet free edges to two reference points below the valve, corresponding to papillary muscle tips.

Because CFD showed wall shear stress is negligible compared with static pressure near the mitral valve [25], only pressure loading was applied: 16 kPa (120 mmHg) on the ventricular wall and leaflet underside [13], and 3333 Pa (25 mmHg) near the aortic valve to represent right ventricular pressure. Maximum systolic pressure was used to estimate upper-bound stress [26]. As left and right ventricular contraction are nearly synchronous [27], both pressures were applied simultaneously. A fixed boundary condition was added at the valve base for stability.

3.3.3. Constitutive Laws

Because the native mitral annulus has a heterogeneous structure and variable collagen content [10], its mechanical behavior is difficult to define. To obtain a conservative estimate, the same Neo-Hookean myocardial parameters were assigned to all biological tissue domains included in the finite element mesh: the lower atrial wall, the upper ventricular wall, the aortic outflow region, the anterior and posterior mitral leaflets, and the atrioventricular junction/annular region. No separate material law was assigned to the annulus or to the leaflets, and no regional fiber orientation was introduced at this stage. This choice was made to obtain a conservative first-order estimate of stress localization, but the resulting stress magnitudes should not be interpreted as definitive tissue failure values. The Neo-Hookean constitutive model uses parameters from existing literature: density 1265 kg/m^3 [28], systolic Young's modulus 300 kPa [29], and Poisson's ratio 0.45 [30].

The prosthetic ring properties were identified by reproducing the Carpentier-Edwards Physio ring compression test in Abaqus [31]. The ring was assumed quasi-incompressible, with density 2300 kg/m^3,

Young's modulus 1.785 MPa, and Poisson's ratio 0.45.

4. RESULTS

4.1. Tissue Deformation Pre- and Post-Surgery

The simulation shows mitral valve deformation caused by prosthetic ring implantation and tightening (see Figure 3, Figure 4 and Table 1). Before the procedure, the annulus is irregular and dilated; after annuloplasty, it becomes more compact due to radial displacement and tissue anchoring. The largest local deformations occur near the anchor sites, where the device imposes the strongest constraints.

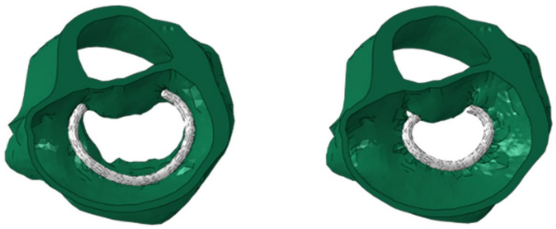

Figure 3. Geometrical top view of the implanted ring on the mitral valve, before (left) and after (right) the annuloplasty procedure.

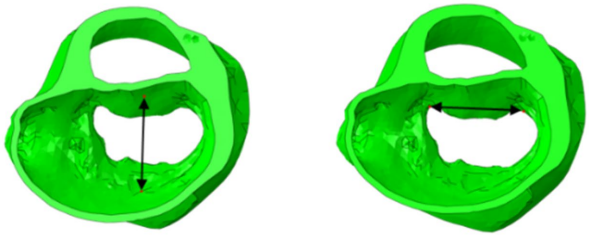

Figure 4. Septal-lateral (SL) distance (left) and commissural-commissural (CC) distance (right) reported between four nodes located on the mitral valve model.

Table 1. The septo-lateral (SL) and commissural-commissural (CC) distances before the downsizing.

	Preoperative	Postoperative	Reduction	Reduction (%)
SL distance [mm]	29.2	24.9	4.3	15%
CC distance [mm]	28.6	22.9	5.7	20%

4.2. Stress Field on the Mitral Annulus and Surrounding Tissues

At each step, the maximum principal stress is evaluated to distinguish between tensile (positive) and compressive (negative) stress states. The thresholds used in the stress maps are post-processing visualization cutoffs only. They were selected to improve figure readability and to isolate the highest-stress regions within each simulation step. They are not tissue damage thresholds, failure criteria, or experimentally validated dehiscence limits. A 140 kPa cutoff was used to highlight broadly stressed regions in the prosthesis-positioning and Physio configurations, whereas a 500 kPa cutoff was used in selected downsizing tensile maps because the stress range was higher.

4.2.1. Prosthesis Positioning (MEP)

As shown in Figure 5, five regions are identified: 1) the prosthetic bed at the atrioventricular junction;

2) the trigones and adjacent ventricular wall; 3) the leaflet free edges; 4) the central anterior leaflet; and 5) the atrial-embedded surface. The maximum principal compressive stress is |402| kPa, and a visualization cutoff of 140 kPa is used to highlight stress sensitive regions.

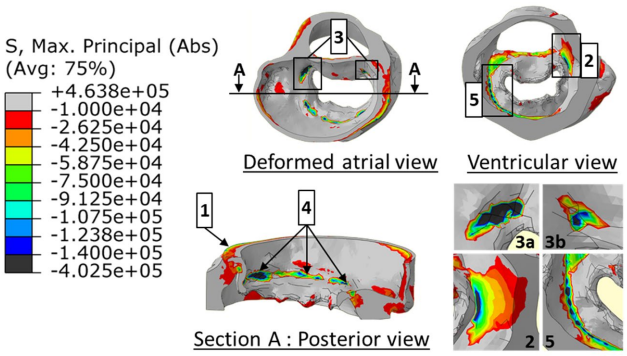

Figure 5. Highly compressed regions are identified in dark grey: 1. the atrial-embedded surface, 2. the left ventricular myocardium near the left trigone, 3. the trigones areas, 4. the prosthesis-valve contact area, and 5. the atrioventricular junction near the P2 and P3 scallops.

As shown in Figure 6, five zones are identified: 1) the commissures; 2) parts of the anterior and posterior leaflets; 3) the atrial cavity surface, excluding the prosthesis contact area; 4) the myocardium; and 5) the aortic wall. The maximum principal tensile stress is 463 kPa, and a visualization cutoff of 140 kPa is used to highlight stress sensitive regions.

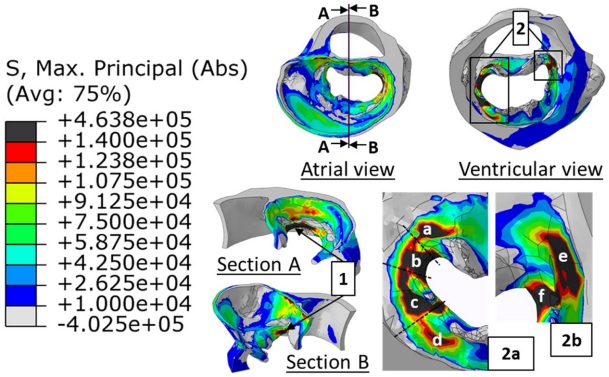

Figure 6. Tensile zones identified with a stress magnitude superior to 140 kPa (dark grey areas): 1. the commissures, 2. the leaflets near the contact zone, and 3. the atrial-embedded surface. a) Right trigone, b) right commissure, c) P3 section of the posterior leaflet, d) P2 section of the posterior leaflet, e) left trigone, and f) left commissure.

4.2.2. Downsizing

As shown in Figure 7, six regions are identified: 1) the ventricular myocardium; 2) the posterior leaflet near the anchors; 3) the inner anterior leaflet and commissural regions; 4) the atrial-embedded surface; 5) the aortic wall; and 6) the inner anchoring surfaces. The maximum principal compressive stress reaches |2.24| MPa at the first anchoring site. Compression within the anchoring surfaces is attributed to the tie constraint between the prosthesis and mitral valve anchors. A steep stress gradient is observed in these areas, indicating that a finer mesh is needed to verify stress magnitude. A visualization cutoff of 140 kPa is used to highlight stress sensitive regions.

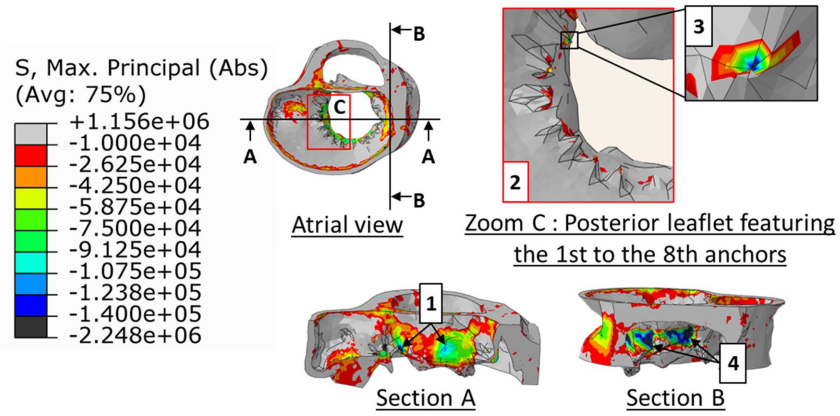

Figure 7. Zones identified with a stress magnitude superior to |140| kPa in compression (dark grey areas): 1. the commissures, 2. the posterior leaflet (P1 and P2 scallops) near the anchors, 3. inside the anchoring surfaces n˚1, 2, 6 and 7, and 4. near the anchors under the leaflets, where the tissue is embedded by the prosthesis.

As shown in Figure 8, four zones are identified: 1) around the anchors; 2) on the atrial cavity surface; 3) in the central anterior leaflet; and 4) near the atrial-embedded interface. The maximum principal tensile stress reaches 1.15 MPa. A visualization cutoff of 500 kPa is used to highlight stress sensitive regions.

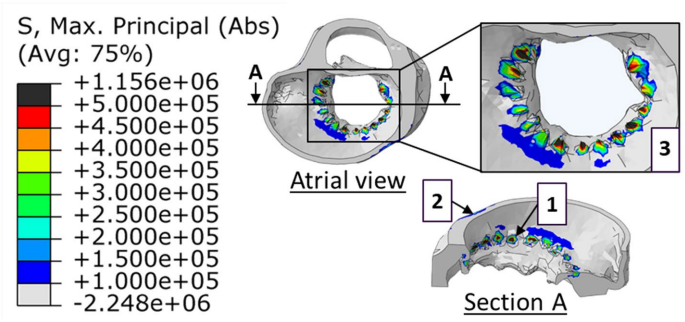

Figure 8. Zones identified with a stress magnitude superior to 500 kPa in traction (dark grey areas): 1. the posterior leaflet (P1 and P2 scallops), 2. near the atrial-embedded surface, and 3. around anchoring sites n˚1, 2, 6, 7, 8, 9, 10, 11, 12, 13 and 14.

For the 14-anchor configuration, post-implantation analysis shows elevated stresses around the mitral annulus, especially near the prosthetic anchors. The highest compressive stresses ($|\sigma| > 1.1$ MPa) occur near the left trigone at the first anchoring site and in the posterior scallops P1 - P2, spanning roughly the first to eighth anchoring sites. Additional tensile stresses ($\sigma > 500$ kPa) are found near the posterior anchoring sites and the atrioventricular junction. These peaks indicate regions potentially more prone to tissue fatigue or suture dehiscence. Overall, posterior and commissural regions show higher stress than anterior zones, consistent with the boundary conditions, anatomy, and regional annular tissue differences.

4.2.3. Physiological Loads: Alternative "Physio" Model

As shown in Figure 9, six regions are identified: 1) the leaflets; 2) the ventricular myocardium near the contraction boundary; 3) the atrial cavity surface; 4) the aortic wall; 5) the chordae tendineae insertion sites; and 6) the atrial-embedded interface. The maximum principal compressive stress reaches |1.19| MPa. A visualization cutoff of 140 kPa is used to highlight stress sensitive regions.

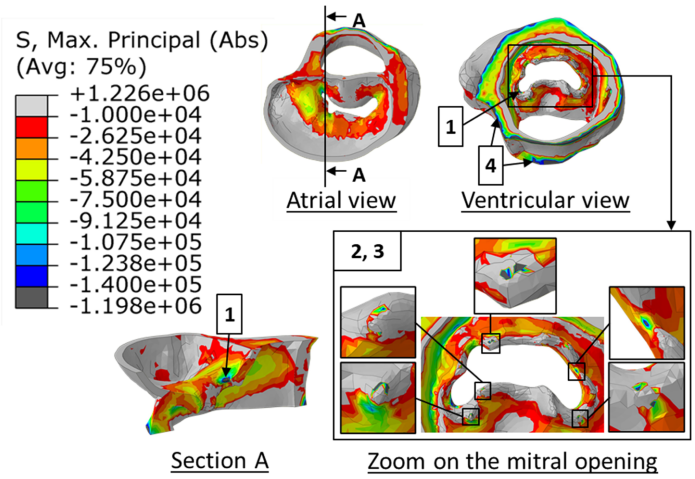

Figure 9. Compressive zones identified with a stress magnitude superior to |140| kPa (dark grey areas): 1. the left commissure, 2. the tendinous chords' insertion sites, 3. the leaflet's free edges, and 4. the atrial embedding.

As shown in Figure 10, five distinct zones are identified under tension: 1) the central region of the anterior leaflet; 2) the chordae tendineae insertion sites; 3) the atrial cavity wall; 4) the atrioventricular junction; and 5) the atrial and ventricular embedded interfaces. The maximum principal tensile stress reaches 1.2 MPa. A visualization cutoff of 140 kPa is used to highlight stress sensitive regions.

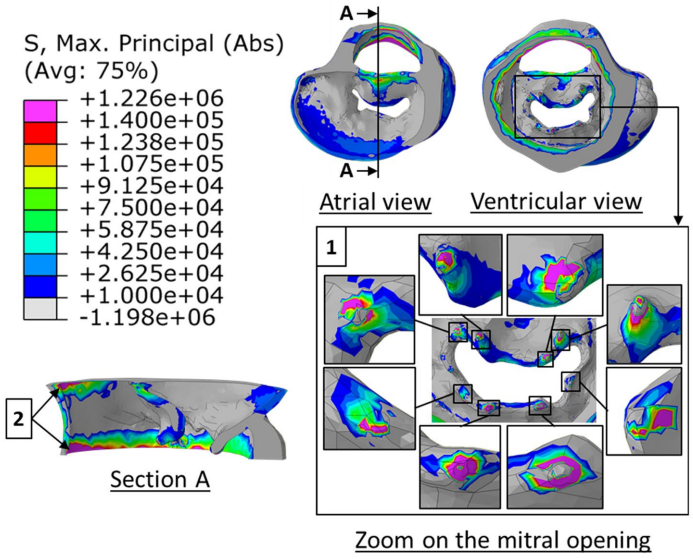

Figure 10. Tensile zones identified with a stress magnitude superior to 140 kPa (lila): 1. the tendinous chords' insertion sites, and 2. the atrial- and ventricular-embedded surface.

4.2.4. Parametric Analysis

If conducted, parametric variations in ring stiffness, ring diameter, and anchor number could clarify the mechanical response of the valve and surrounding tissues. Preliminary results suggest that stiffer rings increase local stress concentrations, whereas more anchoring points may improve load distribution and reduce peak stresses. A comprehensive parametric study is therefore proposed for future work.

5. DISCUSSION

5.1. Comparison with Literature

5.1.1. Reduction Percentage

The percentage reductions in the septal-lateral (SL) and commissure-to-commissure (CC) distances after annuloplasty can be compared with values reported in the literature (see Table 2).

Kong *et al.* [16] quantified reductions in both CC and SL distances following simulated annuloplasty. For a final SL distance of 23.5 mm, they reported a 29.88% reduction. Although they did not report CC diameters below 33.94 mm, they observed an approximate 15% reduction at that diameter.

Wong *et al.* [14] examined dimensional changes after numerical annuloplasty using two ring designs. Starting from an initial SL distance of 14.3 mm, they reported a 7% reduction (to 13.3 mm) with the Physio II ring and a 14% reduction (to 12.3 mm) with the IMR ETlogix ring.

Table 2. Septo-ateral (SL) distances and reductions referred in Kong *et al.* [16], Wong *et al.* [14] and Rausch *et al.* [18] After Annuloplasty (AA).

Kong *et al.*	AA with classic ring (34 mm)	AA with classic ring (36 mm)	AA with GeoForm (36 mm)
SL distance [mm]	29.2	24.9	4.3
SL reduction [%]	28.6	22.9	5.7
Wong *et al.*	Baseline distance (long axis)	AA with Physio II ring (24 mm)	AA with IMR ETlogix ring (24 mm)
SL distance [mm]	14.3	13.3	12.3
SL reduction [%]	-	7	14
Rausch *et al.*	Baseline distance (long axis)	Annular dimension change (24 mm)	Annular dimension change (28 mm)
SL distance [mm]	27.47	23.49	26.66
SL reduction [%]	-	14	3

Our results are of the same order of magnitude, with a 15% reduction in the septal-lateral (SL) distance and a 20% reduction in the commissure-to-commissure (CC) distance. However, they do not exactly match the values reported in the literature. This discrepancy may be partly explained by uncertainty in the placement of measurement points: in the deformed valve geometry, the boundary between the leaflets and the ventricular wall becomes difficult to delineate. Differences in the initial septal-lateral dimension may also contribute to the observed variation.

Downsizing strategies also differ across studies. Rausch *et al.* [18] reported a reduction in SL distance accompanied by an increase in CC distance, reflecting a strategy focused on bringing the anterior and posterior leaflets closer together. In contrast, Kong *et al.* [16] reported reductions in both SL and CC directions.

5.1.2. Stress Distribution

Kong *et al.* reported average/median maximum principal stresses for the anterior and posterior mitral leaflets after annuloplasty and papillary muscle relocation. These quantities are reported for leaflet regions and should not be directly compared with the localized peak stresses obtained in the present study near idealized anchoring and contact constraints. Therefore, the comparison with Kong *et al.* is used here mainly to discuss stress localization trends rather than absolute stress magnitudes. In both studies, the posterior leaflet/annular region appears mechanically more solicited after annuloplasty than other valve regions

A key difference between their approach and ours is the use of an anisotropic hyperelastic constitutive law to represent mitral tissue mechanics. In addition, the leaflets are discretized with hexahedral elements, unlike our meshing strategy. Finally, their simulations employ an explicit formulation, which is often considered less suitable than implicit methods for accurately capturing history-dependent stress responses [16].

In a related numerical study of the mitral valve under physiological loading, Gao *et al.* [17] reported elevated stresses aligned with fiber directions, particularly near the trigones. Their results indicate that the trigonal regions experience higher stress levels than the anterior annulus. Under fully loaded systolic conditions (150 mmHg), the stress at the left trigone reached approximately 193 kPa.

5.1.3. Synthesis of the Literature Comparison

In this study, we developed a mechanically consistent mitral valve model that combines a biofaithful geometry, a Neo-Hookean representation of soft-tissue mechanics, and explicit interaction with a prosthetic annuloplasty ring. The model successfully reproduces the downsizing phase of the procedure. While severe mesh distortion currently limits completion of the subsequent ventricular contraction and hemodynamic loading steps in the full annuloplasty setup, these steps have been robustly implemented and validated in an alternative "Physio" configuration without the prosthesis, providing a clear proof of concept. This establishes a solid foundation for reintegrating physiological loading into the complete annuloplasty framework.

The predicted deformation patterns and stress distributions are coherent with the existing computational literature on annuloplasty. In particular, the concentration of elevated stresses near the fibrous trigones and the posterior annulus is consistent with clinically reported regions prone to suture dehiscence [3, 9]. Likewise, the simulated septo-lateral (SL) reduction agrees with trends reported in the updated Living Heart Model [18] and other finite element studies of mitral valve mechanics [16]. These results support the relevance of the modeling strategy and confirm its ability to capture key mechanical signatures of the procedure.

At this stage, the analysis is based on a single mesh configuration, and a mesh-convergence study is therefore essential to consolidate stress magnitudes and gradients, particularly near anchoring regions. Advancing the model will require a finer discretization and dedicated numerical improvements to control the step-to-step mesh distortions that currently drive convergence issues. Addressing these limitations is a clear and achievable next step, and it will unlock the full predictive potential of the annuloplasty simulation under physiological loading.

5.2. Model Limitation

Several assumptions were necessary given current limitations in available data and computational resources; importantly, each of these choices provides a clear pathway for refinement in future iterations:

The mitral annulus was not segmented directly from patient-specific imaging, but instead reconstructed from adjacent anatomical landmarks. With improved imaging protocols and segmentation workflows, this step can be made fully patient-specific.

The mechanical properties of annular tissue were approximated using myocardial properties. While this may overestimate annular compliance and stress sensitivity, it offers a reasonable baseline that can be updated as more annulus-specific experimental data become available.

Simulations were performed under quasi-static conditions, without explicitly modeling time-varying hemodynamic loads or fatigue behavior. This approach captures the dominant mechanical trends at substantially lower computational cost and establishes a robust foundation for future transient and fatigue-capable analyses.

Anchor-tissue interactions were represented using idealized tie constraints. This provides a stable first-order representation of fixation and can be progressively enriched to include micro-slippage, frictional contact, or detachment criteria as supporting data and calibration targets are introduced.

The chordae tendineae were modeled as one-dimensional spring elements distributed along the free edges of the anterior and posterior leaflets. This simplification captures their main stabilizing effect on leaflet

mechanics, while leaving open the possibility of incorporating a more detailed chordal architecture in subsequent model updates.

Additional factors may also contribute to discrepancies, including uncertainty in generic physiological parameters reported in the literature, the absence of pre-strain, and uncertainty introduced during mitral valve geometry reconstruction and smoothing. Further limitations include the assumption of a purely passive response in the annular and valvular regions and the use of a simplified, isotropic, time-independent elastic material law. Each of these elements represents a well-defined opportunity for improvement and will help strengthen the model's predictive accuracy as the framework evolves.

The validation strategy will be structured in three steps. First, a mesh-convergence study will be performed to assess the robustness of stress magnitudes and gradients near the anchoring regions. Second, the prosthetic ring model will be compared against available compression-test data to verify its effective stiffness. Third, in vitro dehiscence or pull-out tests on representative annular tissue or tissue-mimicking substrates will be used to compare predicted high-stress regions with experimentally observed failure locations. Only after these validation steps will the framework be suitable for stronger predictive or clinical claims.

5.3. Perspectives and Future Work

A parametric study will be conducted in future work to evaluate the influence of ring stiffness, ring diameter, anchor number, and anchor orientation on stress localization. This will allow the sensitivity of the model to procedural and device-design parameters to be quantified systematically.

6. CONCLUSION

6.1. Contribution of This Study

This study presents a finite element model of the mitral valve and surrounding structures designed to investigate the mechanical response of the atrioventricular-junction region during transcatheter annuloplasty. The current model is based on a single reference anatomy and should be considered a methodological framework rather than a fully validated reference anatomical model digital twin.

In the complete annuloplasty model, prosthetic ring positioning and annular downsizing were successfully simulated. Physiological ventricular contraction and pressure loading were implemented separately in a "Physio" configuration without the prosthesis, because severe mesh distortion prevented this loading step from being completed in the downsized prosthesis-including model.

The predicted stress localizations near the fibrous trigones, posterior leaflet region, and atrioventricular-junction region are consistent with trends reported in previous computational studies and with clinically relevant areas for fixation failure. However, the absolute stress magnitudes remain dependent on mesh density, material assumptions, and idealized anchor-tissue constraints. Future work will therefore focus on mesh refinement, validation, and reintegration of physiological loading into the full annuloplasty model.

6.2. Integration into Surgical Planning Tools

This computational framework lays the groundwork for a patient-specific planning tool that could support cardiac surgeons in selecting an appropriate ring size, optimizing anchor placement, and refining the overall implantation strategy. With further development—such as coupling through fluid–structure interaction, incorporating growth and remodeling mechanisms, and enabling near real-time simulations—this virtual platform could be integrated into clinical workflows, helping to improve procedural outcomes and potentially extend prosthesis durability.

ACKNOWLEDGEMENTS

We gratefully acknowledge the support of the Computational Cardiac Modeling group from the Institute of Biomedical Engineering, Karlsruhe Institute of Technology (KIT) for providing the detailed geometry

of the left ventricle used in this study.

The authors also acknowledge that the original imaging modality and acquisition metadata associated with the provided reference geometry were not available to them.

This work was conducted within the Hospital-University Research Program ICELAND and was supported by the French National Research Agency (ANR) under grant ANR-21-RHUS-0006.

DECLARATION

Prior dissemination: A preliminary version of part of this work was presented as an extended abstract at the European Society of Biomechanics (ESB) in 2025. The present manuscript expands that preliminary work by providing a detailed finite element workflow, additional stress analysis, comparison with the literature, clarification of the separate Physio configuration, and an expanded discussion of limitations and validation needs.

CONFLICTS OF INTEREST

The authors declare no conflicts of interest regarding the publication of this paper.

REFERENCES

1. AlQouba, M., AlHumaidi, M., Al Jarallah, M., Dashti, R., Khalil, M., Al Mulla, K., *et al.* (2024) Mitral Regurgitation Quantification, Management, and Guidelines: A 2024 Update. *Annals of Clinical Cardiology*, **6**, 4-16. https://doi.org/10.4103/accj.accj_4_24
2. Carpentier, A. (1983) Cardiac Valve Surgery—The "French Correction". *The Journal of Thoracic and Cardiovascular Surgery*, **86**, 323-337. https://doi.org/10.1016/s0022-5223(19)39144-5
3. Madukauwa-David, I.D., Pierce, E.L., Sulejmani, F., Pataky, J., Sun, W. and Yoganathan, A.P. (2018) Suture Dehiscence and Collagen Content in the Human Mitral and Tricuspid Annuli. *Biomechanics and Modeling in Mechanobiology*, **18**, 291-299. https://doi.org/10.1007/s10237-018-1082-z
4. Estévez-Loureiro, R., Benito-González, T., Garrote-Coloma, C., Fernández-Vázquez, F., Avanzas, P., Piñón, M., *et al.* (2020) Percutaneous Mitral Repair: Current and Future Devices. *Annals of Translational Medicine*, **8**, 963-963. https://doi.org/10.21037/atm.2020.03.154
5. Maisano, F. and Taramasso, M. (2015) The Cardioband Transcatheter Direct Mitral Valve Annuloplasty System. *EuroIntervention*, **14**, W58-W59. https://doi.org/10.4244/eijv11swa15
6. Gasparotti, E., Vignali, E., Mariani, M., Berti, S. and Celi, S. (2022) Image-Based Modelling and Numerical Simulations of the Cardioband® Procedure for Mitral Valve Regurgitation Repair. *Computer Methods in Applied Mechanics and Engineering*, **394**, Article ID: 114941. https://doi.org/10.1016/j.cma.2022.114941
7. Zeng, G., Li, G., Jia, Y., Chen, S., Chen, P. and He, Z. (2021) Detachment Force of the Helical Anchor in Mitral Annulus. *Medicine in Novel Technology and Devices*, **12**, Article ID: 100098. https://doi.org/10.1016/j.medntd.2021.100098
8. Akansel, S., Sündermann, S.H., Kofler, M., Emmerich, A., Falk, V. and Kempfert, J. (2020) Surgical Explantation of a Partially Detached Cardioband Device. *Journal of Cardiac Surgery*, **35**, 2100-2102. https://doi.org/10.1111/jocs.14842
9. Pierce, E.L., Siefert, A.W., Paul, D.M., Wells, S.K., Bloodworth, C.H., Takebayashi, S., *et al.* (2016) How Local Annular Force and Collagen Density Govern Mitral Annuloplasty Ring Dehiscence Risk. *The Annals of Thoracic Surgery*, **102**, 518-526. https://doi.org/10.1016/j.athoracsur.2016.01.107
10. Faletra, F.F., Leo, L.A., Paiocchi, V.L., Caretta, A., Viani, G.M., Schlossbauer, S.A., *et al.* (2019) Anatomy of Mitral Annulus Insights from Non-Invasive Imaging Techniques. *European Heart Journal—Cardiovascular Imaging*,

20, 843-857. https://doi.org/10.1093/ehjci/jez153

11. Gunning, G.M. and Murphy, B.P. (2014) Determination of the Tensile Mechanical Properties of the Segmented Mitral Valve Annulus. *Journal of Biomechanics*, **47**, 334-340. https://doi.org/10.1016/j.jbiomech.2013.11.035
12. Saremi, F., Hassani, C. and Sánchez-Quintana, D. (2016) Septal Atrioventricular Junction Region: Comprehensive Imaging in Adults. *RadioGraphics*, **36**, 1966-1986. https://doi.org/10.1148/rg.2016160010
13. Wright, B.E., Watson, G.L. and Selfridge, N.J. (2020) The Wright Table of the Cardiac Cycle: A Stand-Alone Supplement to the Wiggers Diagram. *Advances in Physiology Education*, **44**, 554-563. https://doi.org/10.1152/advan.00141.2019
14. Wong, V.M., Wenk, J.F., Zhang, Z., Cheng, G., Acevedo-Bolton, G., Burger, M., *et al.* (2012) The Effect of Mitral Annuloplasty Shape in Ischemic Mitral Regurgitation: A Finite Element Simulation. *The Annals of Thoracic Surgery*, **93**, 776-782. https://doi.org/10.1016/j.athoracsur.2011.08.080
15. Wenk, J.F., Zhang, Z., Cheng, G., Malhotra, D., Acevedo-Bolton, G., Burger, M., *et al.* (2010) First Finite Element Model of the Left Ventricle with Mitral Valve: Insights into Ischemic Mitral Regurgitation. *The Annals of Thoracic Surgery*, **89**, 1546-1553. https://doi.org/10.1016/j.athoracsur.2010.02.036
16. Kong, F., Pham, T., Martin, C., Elefteriades, J., McKay, R., Primiano, C., *et al.* (2018) Finite Element Analysis of Annuloplasty and Papillary Muscle Relocation on a Patient-Specific Mitral Regurgitation Model. *PLOS ONE*, **13**, e0198331. https://doi.org/10.1371/journal.pone.0198331
17. Gao, H., Feng, L., Qi, N., Berry, C., Griffith, B.E. and Luo, X. (2017) A Coupled Mitral Valve—Left Ventricle Model with Fluid-Structure Interaction. *Medical Engineering & Physics*, **47**, 128-136. https://doi.org/10.1016/j.medengphy.2017.06.042
18. Rausch, M.K., Zöllner, A.M., Genet, M., Baillargeon, B., Bothe, W. and Kuhl, E. (2016) A Virtual Sizing Tool for Mitral Valve Annuloplasty. *International Journal for Numerical Methods in Biomedical Engineering*, **33**, e02788. https://doi.org/10.1002/cnm.2788
19. Baillargeon, B., Costa, I., Leach, J.R., Lee, L.C., Genet, M., Toutain, A., *et al.* (2015) Human Cardiac Function Simulator for the Optimal Design of a Novel Annuloplasty Ring with a Sub-Valvular Element for Correction of Ischemic Mitral Regurgitation. *Cardiovascular Engineering and Technology*, **6**, 105-116. https://doi.org/10.1007/s13239-015-0216-z
20. Holzapfel, G.A. and Ogden, R.W. (2009) Constitutive Modelling of Passive Myocardium: A Structurally Based Framework for Material Characterization. *Philosophical Transactions of the Royal Society A*: *Mathematical, Physical and Engineering Sciences*, **367**, 3445-3475. https://doi.org/10.1098/rsta.2009.0091
21. Hossien, A., Nithiarasu, P., Cheriex, E., Maessen, J., Sardari Nia, P. and Ashraf, S. (2015) A Multidimensional Dynamic Quantification Tool for the Mitral Valve. *Interactive CardioVascular and Thoracic Surgery*, **21**, 481-487. https://doi.org/10.1093/icvts/ivv187
22. Jeganathan, J., Owais, K., Montealegre-Gallegos, M., Matyal, R., Khabbaz, K. and Mahmood, F. (2016) Dynamic Changes in the Ischemic Mitral Annulus: Implications for Ring Sizing. *Annals of Cardiac Anaesthesia*, **19**, 15-19. https://doi.org/10.4103/0971-9784.173014
23. Chen, S., Sari, C.R., Gao, H., Lei, Y., Segers, P., De Beule, M., *et al.* (2020) Mechanical and Morphometric Study of Mitral Valve Chordae Tendineae and Related Papillary Muscle. *Journal of the Mechanical Behavior of Biomedical Materials*, **111**, Article ID: 104011. https://doi.org/10.1016/j.jmbbm.2020.104011
24. Millard, L., Espino, D.M., Shepherd, D.E.T., Hukins, D.W.L. and Buchan, K.G. (2011) Mechanical Properties of Chordae Tendineae of the Mitral Heart Valve: Young's Modulus, Structural Stiffness, and Effects of Aging. *Journal of Mechanics in Medicine and Biology*, **11**, 221-230. https://doi.org/10.1142/s0219519411003971
25. Daub, A., Kriegseis, J. and Frohnapfel, B. (2020) Replication of Left Ventricular Haemodynamics with a Simple

Planar Mitral Valve Model. *Biomedical Engineering/Biomedizinische Technik*, **65**, 595-603. https://doi.org/10.1515/bmt-2019-0175

26. Kevin, L.G. and Barnard, M. (2007) Right Ventricular Failure. *Continuing Education in Anaesthesia Critical Care & Pain*, **7**, 89-94. https://doi.org/10.1093/bjaceaccp/mkm016
27. Feneley, M.P., Gavaghan, T.P., Baron, D.W., Branson, J.A., Roy, P.R. and Morgan, J.J. (1985) Contribution of Left Ventricular Contraction to the Generation of Right Ventricular Systolic Pressure in the Human Heart. *Circulation*, **71**, 473-480. https://doi.org/10.1161/01.cir.71.3.473
28. Gheorghe, A.G., Fuchs, A., Jacobsen, C., Kofoed, K.F., Møgelvang, R., Lynnerup, N., *et al.* (2019) Cardiac Left Ventricular Myocardial Tissue Density, Evaluated by Computed Tomography and Autopsy. *BMC Medical Imaging*, **19**, Article No. 29. https://doi.org/10.1186/s12880-019-0326-4
29. Huyer, L.D., Montgomery, M., Zhao, Y., Xiao, Y., Conant, G., Korolj, A., *et al.* (2015) Biomaterial Based Cardiac Tissue Engineering and Its Applications. *Biomedical Materials*, **10**, Article ID: 034004. https://doi.org/10.1088/1748-6041/10/3/034004
30. Emig, R., Zgierski-Johnston, C.M., Timmermann, V., Taberner, A.J., Nash, M.P., Kohl, P., *et al.* (2021) Passive Myocardial Mechanical Properties: Meaning, Measurement, Models. *Biophysical Reviews*, **13**, 587-610. https://doi.org/10.1007/s12551-021-00838-1
31. Purser, M.F., Richards, A.L., Cook, R.C., Osborne, J.A., Cormier, D.R. and Buckner, G.D. (2010) A Novel Shape Memory Alloy Annuloplasty Ring for Minimally Invasive Surgery: Design, Fabrication, and Evaluation. *Annals of Biomedical Engineering*, **39**, 367-377. https://doi.org/10.1007/s10439-010-0126-z